Eidgenössische Technische Hochschule Zürich

Ecole polytechnique fédérale de Zurich
Politecnico federale di Zurigo
Swiss Federal Institute of Technology Zurich

Multidimensional method of transport for the shallow water equations

M. Fey[1] and A.-T. Morel

Research Report No. 95-05
June 1995

Seminar für Angewandte Mathematik
Eidgenössische Technische Hochschule
CH-8092 Zürich
Switzerland

[1]Applied Mathematics, California Institute of Technology, Pasadena, CA 91125, USA

Multidimensional method of transport for the shallow water equations

M. Fey[1] and A.-T. Morel

Seminar für Angewandte Mathematik
Eidgenössische Technische Hochschule
CH-8092 Zürich
Switzerland

Research Report No. 95-05 June 1995

Abstract

A truly two-dimensional scheme based on a finite volume discretization on structured meshes will be developed for solving the shallow water equations. The idea of the method of transport, developed by M. Fey for the compressible Euler equations [6], is modified for our case.
In contrast to this, the flux of the shallow water equations is not homogeneous. Hence, the eigenvectors of the Jacobi matrix of the flux can not be used to decompose the state vector. We show that there exist vectors such that the same kind of waves as for the Euler equations can be obtained.
Source terms and appropriate boundary conditions have to be included, to be able to simulate river flow or flow in water reservoirs. Some numerical results will be shown.

Keywords: Shallow water equations, multidimensional waves, dimensional splitting

AMS(MOS) subject classifications (1991): 5M35, 65M06, 76M25, 76B15

[1]Applied Mathematics, California Institute of Technology, Pasadena, CA 91125, USA

1. Introduction

Numerical algorithms for the multidimensional shallow water equations run into the same problems as in the case of the Euler equations. Most of the methods use one-dimensional solvers applied to the different coordinate directions (see [3],[13]). This approach ignores the physical propagation directions and instead uses the coordinate axes, introduced by the underlying grid. This causes a loss of accuracy in regions where the main flow is not aligned with the mesh.
In this paper, we generalize the idea of the method of transport which is a genuine multidimensional scheme [6] to the case of the shallow water equations. This is an example of a conservation law with inhomogeneous flux. Observe that the method of transport for the Euler-equations makes extensive use of the homogeneity of the flux.
In the first part, we describe the model equations and give a brief description of the main idea of the method of transport. Then we derive the proper decomposition of the state vector, leading to a consistent numerical flux. At the end of this paper numerical results of some test problems are shown.

2. Model

In two space dimensions, the differential form of a hyperbolic conservation law looks like:

$$\mathbf{U}_t + \mathbf{F}(\mathbf{U})_x + \mathbf{G}(\mathbf{U})_y = \mathbf{0}. \tag{1}$$

For the shallow water equations we have

$$\mathbf{U} = \begin{pmatrix} h \\ hu \\ hv \end{pmatrix}, \quad \mathbf{F}(\mathbf{U}) = \begin{pmatrix} hu \\ \frac{gh^2}{2} + hu^2 \\ huv \end{pmatrix}, \quad \mathbf{G}(\mathbf{U}) = \begin{pmatrix} hv \\ huv \\ \frac{gh^2}{2} + hv^2 \end{pmatrix}; \tag{2}$$

where h is the depth of the water, g is the constant of gravity, u is the speed in the direction x and v is the speed in the direction y. A simple calculation shows that the flux is not homogeneous, i.e.:

$$\mathbf{F}(\mathbf{U}) \neq \frac{\partial \mathbf{F}(\mathbf{U})}{\partial \mathbf{U}} \mathbf{U}.$$

3. Method of transport

In this section we briefly describe the method of transport and the quantities that need to be replaced in the case of the shallow water equations. For the Euler equations, the numerical scheme relies on the

one-dimensional decomposition of the state vector and the flux in a flux vector splitting way. In the 1-D case, we have

$$\mathbf{F}(\mathbf{U}) = \frac{\partial \mathbf{F}(\mathbf{U})}{\partial \mathbf{U}}\mathbf{U} = \mathbf{R}\Lambda\mathbf{R}^{-1}\mathbf{U} = \sum_{i=1}^{3} \alpha_i \, \mathbf{r}_i \lambda_i, \quad \mathbf{U} = \mathbf{R}\mathbf{R}^{-1}\mathbf{U} = \sum_{i=1}^{3} \alpha_i \, \mathbf{r}_i.$$

The first equalities describe the homogeneity of the flux, where $\mathbf{R}$ denotes the matrix of right eigenvectors of the Jacobian $\partial\mathbf{F}/\partial\mathbf{U}$. Using the second one, we can decompose the state vector into some kind of waves, mainly the eigenvectors times an amplitude. Then the flux is obtained by propagating these waves with their corresponding characteristic speeds. Rearranging these quantities and using the characteristic speed to trace back the propagation we are able to formulate the flux from one domain into another, rather than over cell boundaries. This idea can be applied to several space dimensions in a straightforward way, leading to a multidimensional numerical method [6],[7].
In case of the Euler equations it turns out that the generalization of the eigenvectors $\mathbf{r}_i$, given by

$$\mathbf{R}_1(\mathbf{U}) = \frac{\varrho}{\gamma}\begin{pmatrix} 1 \\ \mathbf{u} \\ H \end{pmatrix}, \quad \mathbf{R}_2(\mathbf{U}) = \frac{\gamma - 1}{\gamma}\varrho\begin{pmatrix} 1 \\ \mathbf{u} \\ |\mathbf{u}|^2/2 \end{pmatrix} \quad \text{and} \quad \mathbf{L}(\mathbf{U}) = \frac{\varrho\, c}{\gamma}\begin{pmatrix} \mathbf{0}^T \\ I \\ \mathbf{u}^T \end{pmatrix}$$

plays an important role. Observe that in general the function $\mathbf{L}(\mathbf{U})$ is a matrix in contrast to the 1-D case. It is the aim of this article to obtain equivalent functions for the shallow water equations.

4. Decomposition

The problem consists of determining the coefficients $\mathbf{R}_1$, $\mathbf{R}_2$ and $\mathbf{L}$. As mentioned before, in the 1-D case the eigenvectors of the Jacobian can not be used. On the other hand, the eigenvectors have no direct physical meaning. Neither do they represent a shock nor a rarefaction wave. But there is no reason not to look for some other vectors with the desired properties. The introduction of the Roe averages is based on the same argument.
In contrast to this, the eigenvalues, i.e. characteristic speeds, are very important for the flow. They indicate the presence of a shock or a smooth flow, whether the characteristics intersect or not.
We construct the matrix $\mathbf{C}_\mathbf{m}$, i.e. the Jacobian of the flux in direction $\mathbf{m} = (\cos\alpha, \sin\alpha)^T$,

$$\mathbf{C}_\mathbf{m} = \frac{\partial \mathbf{F}}{\partial \mathbf{U}}\cos\alpha + \frac{\partial \mathbf{G}}{\partial \mathbf{U}}\sin\alpha$$

or explicitly

$$\mathbf{C_m} = \begin{pmatrix} 0 & \cos\alpha & \sin\alpha \\ (g\,h - u^2)\cos\alpha - u\,v\sin\alpha & 2\,u\cos\alpha + v\sin\alpha & u\sin\alpha \\ -u\,v\cos\alpha + (g\,h - u^2)\sin\alpha & v\cos\alpha & u\cos\alpha + 2\,v\sin\alpha \end{pmatrix}$$

with the eigenvalues

$$\begin{aligned} \lambda_{1,3} &= u\cos\alpha + v\sin\alpha \pm \sqrt{gh} = \mathbf{u}\cdot\mathbf{m} \pm c, \\ \lambda_2 &= u\cos\alpha + v\sin\alpha = \mathbf{u}\cdot\mathbf{m}. \end{aligned}$$

Here $\mathbf{u} = (u, v)^T$ is the velocity. It is easy to verify that

$$\mathbf{C_m U} \neq \mathbf{F}(\mathbf{U})\cos\alpha + \mathbf{G}(\mathbf{U})\sin\alpha.$$

The idea is to find a matrix $\mathbf{A}(\mathbf{U})$ such that $\mathbf{A}(\mathbf{U})$ is similar to $\mathbf{C_m}$ and $\mathbf{A}(\mathbf{U})\mathbf{U} = \mathbf{F}(\mathbf{U})\cos\alpha + \mathbf{G}(\mathbf{U})\sin\alpha$.
Since $\mathbf{A}(\mathbf{U})$ is similar to $\mathbf{C_m}$, there exists a matrix $\mathbf{R}$ such that

$$\mathbf{F}(\mathbf{U})\cos\alpha + \mathbf{G}(\mathbf{U})\sin\alpha = \mathbf{R}\Lambda\mathbf{R}^{-1}\mathbf{U}.$$

This leads to 3 equations in 9 unknowns in the 2-D case. Three free parameters reflect the freedom of length for each eigenvector. The other three can be fixed by comparison with the 1-D case where the solution is unique. Some algebra leads to the eigenvectors $\mathbf{r}_1$, $\mathbf{r}_2$ and $\mathbf{r}_3$ of $\mathbf{A}(\mathbf{U})$, given by

$$\mathbf{R} = (\mathbf{r}_1, \mathbf{r}_2, \mathbf{r}_3) = \begin{pmatrix} 1 & 0 & 1 \\ u + \dfrac{\sqrt{gh}\cos\alpha}{2} & -\sin\alpha & u - \dfrac{\sqrt{gh}\cos\alpha}{2} \\ v + \dfrac{\sqrt{gh}\sin\alpha}{2} & \cos\alpha & v - \dfrac{\sqrt{gh}\sin\alpha}{2} \end{pmatrix},$$

and thus $\mathbf{A}(\mathbf{U})$ has the form

$$\begin{pmatrix} -u\cos\alpha - v\sin\alpha & 2\cos\alpha & 2\sin\alpha \\ \dfrac{gh\cos\alpha}{2} - 2u^2\cos\alpha - 2uv\sin\alpha & 3u\cos\alpha + v\sin\alpha & 2u\sin\alpha \\ \dfrac{gh\sin\alpha}{2} - 2uv\cos\alpha - 2v^2\sin\alpha & 2v\cos\alpha & u\cos\alpha + 3\,v\sin\alpha \end{pmatrix}.$$

The eigenvectors of $\mathbf{A}(\mathbf{U})$ and $\mathbf{C_m}$ differ only in the divisor 2 in the term with $g\,h$. Using this, the amplitude α_i of the waves can be calculated as

$$\begin{pmatrix} \alpha_1 \\ \alpha_2 \\ \alpha_3 \end{pmatrix} = \mathbf{R}^{-1}\,\mathbf{U} = \frac{h}{2}\begin{pmatrix} 1 \\ 0 \\ 1 \end{pmatrix}.$$

Guided by the one-dimensional case, where

$$\mathbf{R_1}(\mathbf{U}) = \alpha_1 \mathbf{r}_1 + \alpha_3 \mathbf{r}_3 = h \begin{pmatrix} 1 \\ u \\ v \end{pmatrix} \quad \text{and} \quad \mathbf{L}(\mathbf{U}) = \alpha_1 \mathbf{r}_1 - \alpha_3 \mathbf{r}_3 = \frac{hc}{2} \begin{pmatrix} 0 \\ \cos\alpha \\ \sin\alpha \end{pmatrix},$$

we define

$$\mathbf{R_1}(\mathbf{U}) = h \begin{pmatrix} 1 \\ \mathbf{u} \end{pmatrix} \quad \text{and} \quad \mathbf{L}(\mathbf{U}) = \frac{hc}{2} \begin{pmatrix} \mathbf{0}^T \\ \mathbf{I} \end{pmatrix}$$

for the multidimensional case. Again, $\mathbf{L}(\mathbf{U})$ now becomes a $(N+1) \times N$ matrix, as in the Euler case.
It turns out that $\mathbf{R_2}(\mathbf{U}) = \alpha_2 \mathbf{r}_2 = \mathbf{0}$ vanishes completely, i.e. there is no advection wave for the shallow water equations.
With this decomposition we are now able to compute the fluxes $\mathbf{F}_{\Omega_i\Omega_j}$ as the integrals of the waves generated by domain Ω_i over the domain Ω_j. Corresponding to [6] we get

$$\mathbf{F}^{c}_{\Omega_i\Omega_j} = \int_{\Omega_j} \frac{1}{|O|} \int_O \int_{\Omega_i} \mathbf{R}_1(\mathbf{U}(\mathbf{y},t))\, \delta(\mathbf{x} - \mathbf{g}(\mathbf{y},t,\Delta t)) d\mathbf{y} dO d\mathbf{x}$$

$$\mathbf{F}^{c^-}_{\Omega_i\Omega_j} = \int_{\Omega_j} \frac{N}{|O|} \int_O \int_{\Omega_i} \mathbf{L}(\mathbf{U}(\mathbf{y},t)) \cdot \mathbf{n}\, \delta(\mathbf{x} - \mathbf{g}(\mathbf{y},t,\Delta t)) d\mathbf{y} dO d\mathbf{x}$$

and $\mathbf{F}_{\Omega_i\Omega_j} = \mathbf{F}^{c}_{\Omega_i\Omega_j} + \mathbf{F}^{c-}_{\Omega_i\Omega_j}$. The update for the new timestep is done by adding incoming and subtracting outgoing fluxes. We obtain

$$\mathbf{U}_i^{n+1} = \mathbf{U}_i^n - \frac{1}{|\Omega_i|} \sum_{j \neq i} (\mathbf{F}_{\Omega_i\Omega_j} - \mathbf{F}_{\Omega_j\Omega_i}) = \frac{1}{|\Omega_i|} \sum_j \mathbf{F}_{\Omega_j\Omega_i}, \tag{3}$$

where i is the index of the central cell and in the first sum the index j runs over the indices of all neighboring cells. E.g. for a Cartesian grid in two space dimensions, the flux of the 8 nearest neighbors has to be taken into account. The above description of the flux can be used for the method of transport, but usually we are using a simplified method of transport, where the fluxes are an approximation of the ones mentioned above [5].

5. Examples

5.1. **Circular expansion.** Solving a spherical symmetric problem on a Cartesian mesh causes a lot of problems for any kind of numerical method as shown in [11] for the Euler equations. To show the multidimensional character of the method, we compare the results of a circular expansion with the solutions of a first order van Leer flux vector splitting scheme.

We consider a square domain $[-1,1] \times [-1,1]$ with initial conditions

$$h(\mathbf{x},0) = \begin{cases} h_i \text{ if } ||\mathbf{x}|| \leq 0.3 \\ h_e \text{ if else} \end{cases} \tag{4}$$

and $\mathbf{u}(\mathbf{x},0) = 0$. A uniform grid with 160 points in each direction is used.

First we found that the method of transport (MoT) gives results for CFL-number up to unity, whereas for the robust van Leer method (VLM) in dimensional splitting, the maximum CFL-number was restricted to $CFL < 0.7$. Hence, we used the constant timestep $\Delta t = 1.9 \cdot 10^{-3}$ in all computations.

In this example the Froude number is always less than 1.7 so that the subsonic, transonic and supersonic propagation, i.e. propagation in all directions, are to be considered. The two contour plots of the water depth in Fig. 1 show the influence of the Cartesian grid. For the VLM, thickness and position of the front shock depend on the direction. Conversely, the MoT gives an almost symmetric solution with no dependence on the shape of the front shock or on the direction. Fig. 2 shows cuts along the x-axis and Fig. 3 along the diagonal to the grid. The slowest front shock in the cuts along the x-axis and along the diagonal belong to the VLM.

The simplified method as proposed in [5] runs also in this example. The discretization is still stable up to $CFL = 1$. But the resolution of the sonic point is not so good, we noticed the occurrence of glitches in

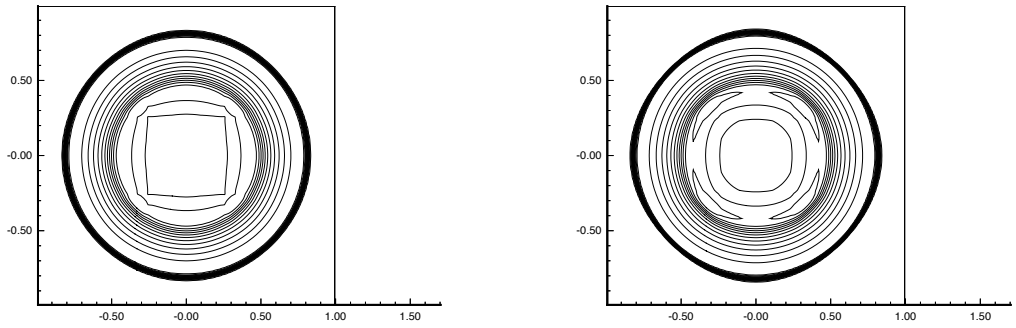

FIGURE 1. Wave in a square domain (160×160) satisfying the initial conditions with $h_i = 1.0$ and $h_e = 0.1$, contour lines of the depth after 100 steps computed with MoT (left) and VLM (right), with $\Delta t = 1.9 \cdot 10^{-3}$.

these regions. This is a well known problem for the Steger-Warming splitting [2].

5.2. **Shock formation.** We consider the flow along an oblique corner of angle $\pi - \theta$ (see Fig. 4). The incoming parallel flow is reflected at the wall and produces a shock. For this example, an analytical solution for the shock angle exists [1]. Let u_1 and u_2 be the speed of the water on each side of the shock. Since the velocity component parallel to the shock is continuous, we get $u_1 \cos\beta = u_2 \cos(\beta - \theta)$ and $\tan(\beta - \theta)/\tan\beta = (u_2 \sin(\beta - \theta))/(u_1 \sin\beta)$.

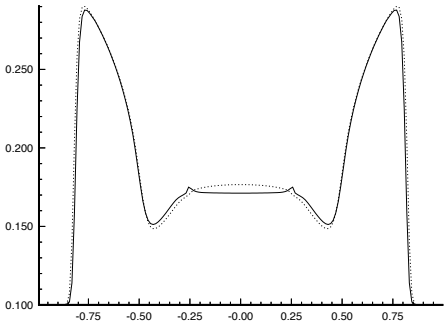

FIGURE 2. Cuts along the planes $y = 0$ for the previous contour plots. The solid line is the result of MoT, the doted line is from VLM.

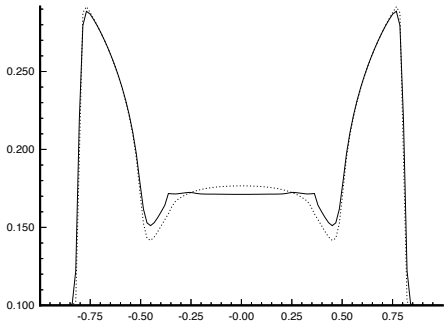

FIGURE 3. Cuts along the planes $y = x$ for the previous contour plots. The solid line is the result of MoT, the doted line is from VLM.

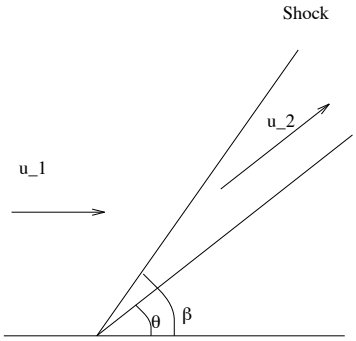

FIGURE 4. Geometry for example 2.

Using the Rankine-Hugoniot condition, the reflection angle is given by

$$\tan\theta = \frac{(1-L)\tan\beta}{1+L\,\tan^2\beta} \tag{5}$$

where

$$L = \frac{1+\sqrt{1+8\,(Fr)^2\sin^2\beta}}{4\,(Fr)^4\sin^2\beta} \qquad \text{and} \qquad Fr = \frac{u}{\sqrt{g\,h}}.$$

Fr is the Froude number in the x direction in the free stream.
In the example we set the wall angle to 45° and $h = 0.096$ and $Fr = 6$ in the free stream region. We calculated the solution on a uniform Cartesian grid (80×80) after 300 time steps with $\Delta t = 1.2267 \cdot 10^{-3}$. Uniform free stream values were taken as initial conditions. The numerical reflection angle is 58.35° compared to 58.63° as theory predicts.

5.3. **Expansion in a channel.** We compare the numerical results of the expansion of water in a channel with experiments. Hager and Mazumder [9] measured the supercritical flow at abrupt expansions in a channel of length 8 meter and width 1.5 meter. The opening is one third of the total width and the flow arrives with a height of 0.096 meter and a Froude number of 3.
The stationary solution shows the same structure as the measurements, but in the simulation all lines are shifted downstream. The inclusion of friction corresponding to the bed shear stress to the model, leads to the correct solution (see Fig. 5).
The friction can be added to the equations by a source term

$$\mathbf{S}(\mathbf{U}) = \begin{pmatrix} 0 \\ -g\,h\,S_{f_x} \\ -g\,h\,S_{f_y} \end{pmatrix},$$

where S_{f_x} and S_{f_y} are the slopes of the energy grade lines in the x and y directions respectively. The values are given by the steady state friction formulae $S_{f_x} = (n^2\,u\,\sqrt{u^2+v^2})/h^{4/3}$ in which n is Manning's roughness coefficient. In each step we use an operating splitting, i.e. we first solve the homogeneous equations (1) and than the ordinary differential equations $\mathbf{U}_t = \mathbf{S}(\mathbf{U})$. Since in this example the source term is not stiff, the operating splitting causes no problems [4].

6. Conclusion

We were able to derive a multidimensional method for a hyperbolic system of partial differential equations with non homogeneous flux. As shown in the numerical examples, the physics is correctly represented with almost no dependence on the grid. Adaptions to special features

of the equations are necessary to obtain efficient numerical methods. This includes the reduction of numerical viscosity, due to the lack of an advection part, as well as a high order implementation of this method. The latter is possible as shown in [8] in the case of the Euler equations.

References

1. J. D. Anderson. *Modern Compressible Flow*. McGraw-Hill Book Company, New-York, 1982.
2. W.K. Anderson, J.L. Thomas, B. van Leer. A Comparison of Finite Volume Flux Vector Splittings for the Euler Equations, *AIAA* 85-0122, 1982.
3. R. J. Fennema and M. H. Chaudhry. Explicit Methods for 2-D Transient Free-Surface Flows. *Jour. of Hydraulic Engineering*, 1990, **116**, Aug., 1013-1034.
4. M. Fey, H. Jarausch, R. Jeltsch and P. Karmann. On the Interaction of Euler and ODE Solver when Computing Reactive Gas Flow, *Proceedings of the Workshop on Adaptive Computational Methods for Partial Differential Equations*, SIAM, 1988.
5. M. Fey and R. Jeltsch. A simple multidimensional Euler scheme, *Proceedings of the First European Computational Fluid Dynamics Conference, Brussels, 7-11 September 1992*, Elsevier Science Publishers, 1992.
6. M. Fey. *Ein echt mehrdimensionales Verfahren zur Lösung der Eulergleichungen*. Dissertation, ETH Zürich, 1993.
7. M. Fey. A genuinely Multidimensional Method to solve the Euler Equations. Submitted to *J. Comp. Phys.*, 1994.

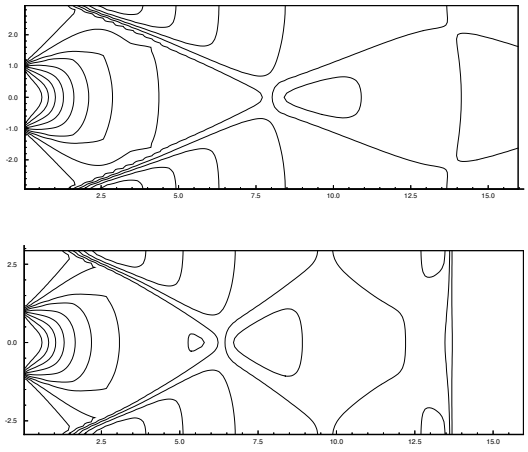

FIGURE 5. Flow in expansion for $h_0 = 96$ mm, $Fr_0 = 3$ on a domain (240×45). Plotted are the contour lines of h/h_0, after 1000 steps with $\Delta t = 1.00 \cdot 10^{-3}$ without source term (upper figure) and with source term (lower figure).

8. M. Fey. Multidimensional High Order Schemes for Systems of Conservation Laws, submitted to *Proceedings of the Fifth International Conference on Hyperbolic Problems*, Stony Brook, 1994.
9. W. H. Hager and S. K. Mazumder. Supercritical flow at abrupt expansions. *Proc. Instn Civ. Engrs Wat., Marit. and Energy*, 1992, **96**, Sept., 153-166.
10. R. J. LeVeque. *Numerical Methods for Conservation Laws*. Birkäuser, Basel, 1990.
11. R. J. LeVeque and R. Walder. Grid Alignment Effects and Rotated Methods for Computing Complex Flows in Astrophysics, *Proceedings of the 9th GAMM Conference on Numerical Methods in Fluid Dynamics, Notes on Numerical Fluid Mechanics*, Vieweg Verlag, 1991.
12. B. Van Leer. Flux vector splitting for the Euler equations. *Proc. 8th International Conference on Numerical Methods in Fluids Dynamics*, Springer Verlag, Berlin, 1982.
13. J. Y. Yang and C. A. Hsu. Computation of free surface flows (part 2). *Jour. of Hydraulic Research*, 1993, **31**, No. 3, 403-414.

Research Reports

No.	Authors	Title
95-05	M. Fey, A.-T. Morel	Multidimensional method of transport for the shallow water equations
95-04	R. Bodenmann, H.J. Schroll	Compact difference methods applied to initial-boundary value problems for mixed systems
95-03	K. Nipp, D. Stoffer	Invariant manifolds and global error estimates of numerical integration schemes applied to stiff systems of singular perturbation type - Part II: Linear multistep methods
95-02	M.D. Buhmann, F. Derrien, A. Le Méhauté	Spectral Properties and Knot Removal for Interpolation by Pure Radial Sums
95-01	R. Jeltsch, R. Renaut, J.H. Smit	An Accuracy Barrier for Stable Three-Time-Level Difference Schemes for Hyperbolic Equations
94-13	J. Waldvogel	Circuits in Power Electronics
94-12	A. Williams, K. Burrage	A parallel implementation of a deflation algorithm for systems of linear equations
94-11	N. Botta, R. Jeltsch	A numerical method for unsteady flows
94-10	M. Rezny	Parallel Implementation of ADVISE on the Intel Paragon
94-09	M.D. Buhmann, A. Le Méhauté	Knot removal with radial function interpolation
94-08	M.D. Buhmann	Pre-wavelets on scattered knots and from radial function spaces: A review
94-07	P. Klingenstein	Hyperbolic conservation laws with source terms: Errors of the shock location
94-06	M.D. Buhmann	Multiquadric Pre-Wavelets on Non-Equally Spaced Centres
94-05	K. Burrage, A. Williams, J. Erhel, B. Pohl	The implementation of a Generalized Cross Validation algorithm using deflation techniques for linear systems
94-04	J. Erhel, K. Burrage, B. Pohl	Restarted GMRES preconditioned by deflation
94-03	L. Lau, M. Rezny, J. Belward, K. Burrage, B. Pohl	ADVISE - Agricultural Developmental Visualisation Interactive Software Environment
94-02	K. Burrage, J. Erhel, B. Pohl	A deflation technique for linear systems of equations
94-01	R. Sperb	An alternative to Ewald sums
93-07	R. Sperb	Isoperimetric Inequalities in a Boundary Value Problem in an Unbounded Domain